J Electroceram (2009) 22:209–215
DOI 10.1007/s10832-007-9334-9

Low temperature cofirable MnZn ferrite for power electronic applications

Richard Matz · Dieter Götsch · Roman Karmazin · Ruth Männer · Bernhard Siessegger

Received: 5 March 2007 / Accepted: 12 September 2007 / Published online: 26 September 2007

Abstract A new MnZn ferrite tape material for sintering at 900 °C and its performance in power electronic embedded multilayer inductors of several μH inductance are described. The low sintering temperature is achieved by optimizing powder processing and sintering additives. The material is suited for processing within the low temperature cofired ceramics (LTCC) technology and it is particularly compatible with low loss Ag metallization. Although reduced by a factor of two compared to high-temperature sintered material, its relative amplitude permeability of 700 allows for numerous device applications below the Curie temperature of 260 °C. Volumetric losses are not affected by the new material formulation since increased hysteresis losses are compensated by reduced eddy current losses. Power line filters with ceramic integrated inductors and surface mounted capacitors exhibit a current capacity of up to 10 A and a shift in cutoff frequency compatible with the measured *B–H* curve of the material. By integration of these inductors with conventional dielectric LTCC tapes a strain-induced permeability quenching is revealed and attributed to magnetostriction. Therefore good thermal matching between tape materials is needed, but the effect also permits construction of variometers and pressure sensors without moving mechanical parts.

Keywords Low temperature cofired ceramics · MnZn ferrite · Passive integration · Inductor · Line filter

R. Matz (✉) · D. Götsch · R. Karmazin · R. Männer · B. Siessegger
Siemens Corporate Technology,
81730 Munich, Germany
e-mail: richard.matz@siemens.com

1 Introduction

Electronic components miniaturization remains with the enabling technologies of mobile, intelligent and modular subsystems. As such it is spreading from semiconductors into printed circuit boards and assembly and interconnect technologies. However, the chances and the susceptibility to this trend differ widely among the technologies and devices. Due to the intricacy of magnetic fields and materials, particularly inductive components have long been subject to ongoing miniaturization efforts. In the microwave regime, useful impedances are associated with relatively small inductances of several nH; the development aimed to integrate these naturally small components on silicon with sufficient self resonant frequencies and quality factors, e.g. by separating solenoidal or spiral coils from the lossy substrate [1, 2]. In power electronics, however, as for example power converters, lamp ballasts and switched mode power supplies current amplitudes are higher and frequencies of operation are correspondingly lower by a few orders of magnitude. Inductors have μH size now and must be placed off-chip. As they form a functional unit with the active devices and can be an integral part of the package, the term system-in-package has been coined. The most obvious approach is the integration of surface mounted discrete devices into the printed circuit board (PCB) by use of suitable ferrite materials; e.g. ferrite polymer compound layers [3] and electroplated NiFe layers [4] were employed to demonstrate a 60 W transformer and a DC–DC converter with PCB-integrated inductor, respectively. Besides integration, also multiple use of a conventional discrete ferrite core may be an approach to reduce size and cost [5].

Since higher inductance values require the use of ferrites to enhance the magnetic flux density, the high temperature

processing of ceramic multilayer boards is of great advantage to make more high-end materials available for integration than are possible within the low temperature processing window of organic circuit boards. In standard LTCC technology, ceramic green tapes are processed by punching and screen printing to form vertical interconnects and planar conductor patterns; a multitude of tapes is finally laminated and sintered at 900 °C to form a hermetically sealed, robust ceramic multilayer circuit board. Sintering additives like various glasses are used to reduce the sintering temperature to below the melting point of Ag, a major constituent of common metallization pastes. Ba hexaferrites were recently adapted to LTCC for microwave applications [6, 7] but NiCuZn ferrites have found even more interest due to their good processability and performance up to several 10 MHz. Relative permeabilities of up to 400 and inductances of several 100 μH were reported [8]. The high inductance per unit length exhibited by ferrite-embedded conductors also facilitates inductors with simultaneously high current capacity; e.g. 4.7 μH with 0.8 A [9] or 20 nH with 20 A [10] were achieved for DC–DC converters. Besides the versatile finite element modeling (FEM) design approach also analytical formulas are available for inductances of planar coils on top of [11] or embedded into [12] ferromagnetic substrates. Coupling between embedded inductors was found to be reduced by the immediate low reluctance path around each conductor, which enforces countermeasures and tradeoffs in the structural design of planar integrated transformers [13–15].

It is the intention of the present work to further extend LTCC technology by adding low temperature sintered MnZn ferrite tapes. MnZn ferrite is one of the most used materials for power applications in the lower MHz regime like switched mode power supplies. It promises higher permeability than NiCuZn ferrite, however at lower gyromagnetic resonance frequency and the need to control the oxygen partial pressure during sintering. After a description of the adaptation procedure of the material and its resulting properties an embedded multilayer inductor will be considered as part of a power line filter including aspects of combination with dielectric tapes and current capacity.

2 Material synthesis and characterization

As an established soft ferrite for power transformers and inductors offering high initial permeability and magnetic saturation, MnZn ferrite is also an interesting candidate for LTCC. As compared to NiZn ferrite, its drawbacks like low specific resistivity, high permittivity and sensitivity to excess oxygen during sintering can be overcome by device design and process control. Usually, the powder is calcinated between 800 and 900 °C and sintered after addition of binder and sintering aids in shaped form between 1100 and 1300 °C in nitrogen atmosphere with controlled oxygen partial pressure. For LTCC, we use these final sintering conditions for the initial calcination of commercially available ferrite powders [16] and reduce the sintering temperature accordingly to 900 °C in nitrogen after binder burnout in air. To boost sintering activity, however, an additional high energy milling step is applied to the powder after the high temperature calcination and prior to mixing with sintering aids.

The resulting microstructure is revealed by the scanning electron micrograph (SEM) in Fig. 1. Most of the material consists of the MnZn-rich phase into which a few Fe-rich grains are embedded. The Bi_2O_3–B_2O_3–SiO_2–ZnO glass (BBSZ) used as sintering aid in an amount of a few volume % segregates at the grain boundaries. The porosity is typically around 2%. The complex initial permeability was determined from bulk and tape ring cores with ten turns of Cu wire by impedance analysis (HP4194A) between 0.5 and 20 MHz. Up to 6 MHz we find μ' between 500 and 600, i.e. about a factor of two below that of commercial, high temperature sintered ferrite. The resonance frequencies ($\tan\delta=\mu''/\mu'=1$) of LTCC bulk and tape material are 6 and 15 MHz, respectively, and the Curie temperature is 260 °C.

Since grain boundaries impede the domain wall movement, a grain size of at least several μm was found to be necessary for good magnetic performance. A glass content above 5 vol.% is similarly detrimental. Since the macroscopic specific resistivity is determined by the grain boundary composition, however, the glass phase helps to improve the material's performance: Specific DC resistivities above 1 kΩ·m were found while standard material

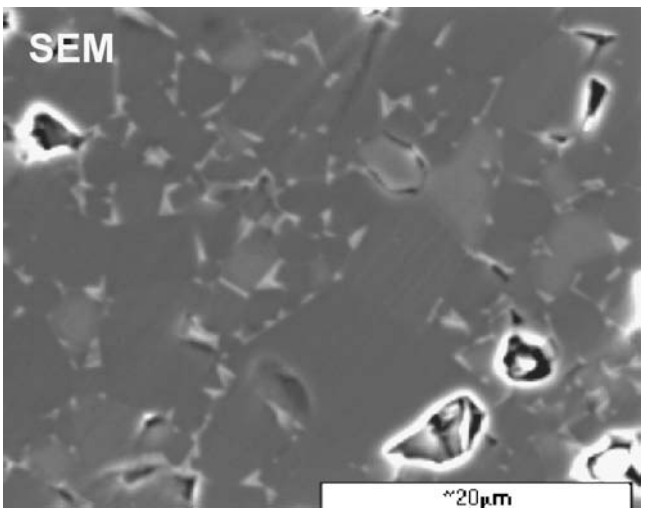

Fig. 1 Scanning electron micrograph (SEM) of ferrite grain structure revealing *dark grey* MnZn rich and *light grey* Fe rich phases as well as Bi–B–Si–Zn glass (*white*) at the grain boundaries

typically exhibits a few Ω·m [17]. At 2.5 MHz the loss tangent amounts to 0.15 and does not exhibit any pronounced dependence on grain size or glass content. This is attributed to compensation effects as larger grains permit better magnetic interaction and reduce the hysteresis loss while smaller grains with insulating glass-filled grain boundaries reduce the eddy current loss.

A sinus signal generator (Rohde&Schwarz, SMY 01), power amplifier (Amplifier Research Model 250L), and digitizing oscilloscope (Tektronix TDS 520A) were employed to measure amplitude permeability, specific loss and hysteresis by analyzing the current and voltage time signals of the ring cores. The Figs. 2 and 3 show results at various frequencies. The cutoff in the amplitude permeability reveals magnetic saturation occurring at lower flux density for higher frequency. Losses include hysteresis loss, eddy current loss and resonance loss; they increase in a quadratic manner with flux density. Comparing to commercial 3F4 material [17] at 2.5 MHz and low flux, neither the total specific loss nor the amplitude permeability are appreciably deteriorated by the modifications in composition and processing; however, magnetic saturation occurs at a lower flux of about 40 mT (2.5 MHz). This is attributed to the reduced density of the magnetic phase in LTCC material.

Similar behaviour is evident from the magnetic hysteresis curves at the low frequency of 100 kHz in Fig. 4. Due to the content of sintering additives and foreign phases as well as the smaller grains the permeability and the magnetic saturation are reduced while the coercive field and the hysteresis loss (=area enclosed) are increased. Grain growth is particularly impeded by the layer interfaces in the multilayer tape sample. The hysteresis shrinks to an ellipse for 2.5 MHz which indicates a loss of 5.3 W/cm^3 for 40 mT peak flux density (Table 1). The specific total loss was found to be 6.6 W/cm^3 under these conditions, i.e. 20 °C and 40 mT (lower than shown in Fig. 3 for 100 °C). The difference of 1.3 W/cm^3 is due to eddy currents and magnetic resonances. However, the eddy current loss appears negligible according to theory for ferrite dimensions in the millimetre range, even for the largest reasonable conductivity of 1 S/m.

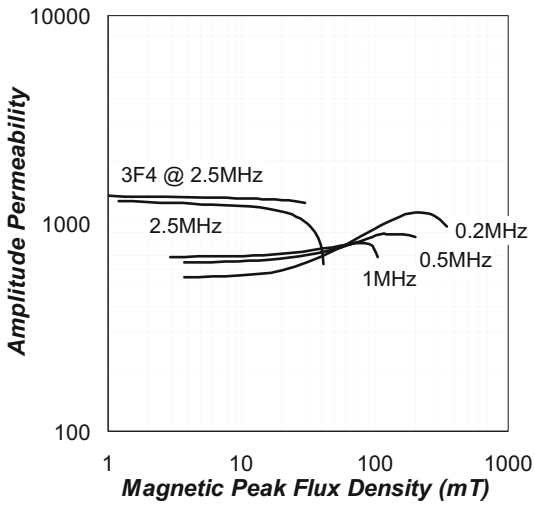

Fig. 2 Amplitude permeability of sintered LTCC MnZn ferrite tape in relation to commercial 3F4 material measured at 100 °C

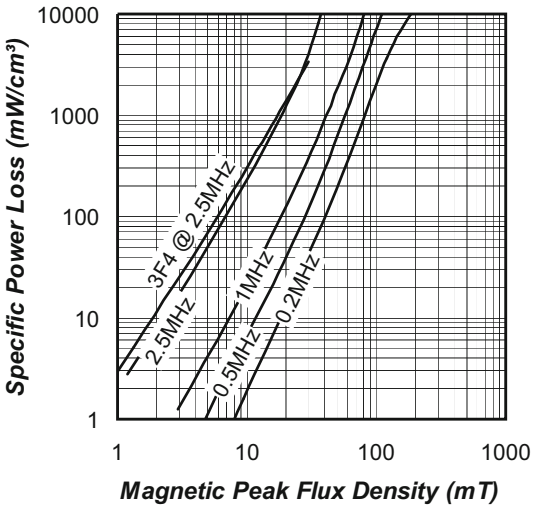

Fig. 3 Volumetric power loss of sintered LTCC MnZn ferrite tape in relation to commercial 3F4 material measured at 100 °C

3 Multilayer inductor for power line filter

The inductance per unit length of an embedded conductor line is proportional to the permeability of the surrounding material as long as a sufficient material thickness is provided. This could be confirmed both experimentally and by FEM [19]. The latter also revealed that the magnetic flux closes immediately around the conductor due to the low reluctance path provided by ferrite material. Multiple

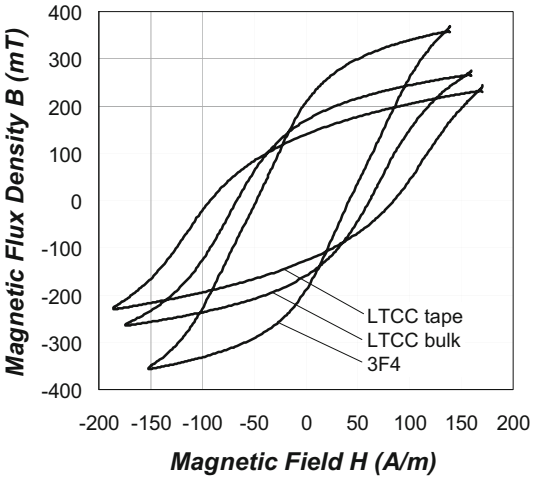

Fig. 4 Magnetic hysteresis of sintered LTCC MnZn ferrite bulk and tape material in relation to commercial 3F4 material at 100 kHz

Table 1 Analysis of magnetic losses (in W/cm^3) of MnZn ferrite LTCC tapes.

Type of loss	Source	Value
Total	Measured at 20 °C (similar to Fig. 3)	6.6
Hysteresis	Measured at 20 °C	5.3
Eddy current	Calculated from $(\pi^2/6)\sigma\, d^2\, \widehat{B}^2\, f^2$ [18] with σ=1 S/m, d=1 mm, f=2.5 MHz	0.01
Resonance	Total–hysteresis–eddy current	1.3

turns of a coil are therefore not magnetically coupled and the inductance is simply proportional to the length of conductor rather than the square of the number of turns. For example, a single oval turn was embedded between five ferrite bottom and top layers for a 2.2μH inductor. The conductor of 500μm width and 20 mm length consisted of two parallel lines on top and bottom of a central ferrite layer to enhance the current capacity. Hence, the total layer count was 11 and the sample volume was 11.3×6.5×1.0 mm^3. Although standard AgPd metallization performed well with the longest ferrite sintering times, the design goal of high current capacity enforced pure Ag metallization. Metal stability combined with ferrite performance was achieved by reducing the sintering time to below 10 h. Two shunt capacitors of 3×3.3 μF each were surface mounted after firing to form a low-pass filter. The layout (Fig. 5) is designed such that a large rectangular electrode in the upper half exists on front and back side to provide signal input and output ports, both being connected by the internal coil. Symmetric ground electrodes in the lower half are connected to each other by a via fence. These structures are also clearly recognizable in the photograph of the sintered plate in Fig. 6.

The inductor has been characterized in an impedance analyzer (HP4194A) both as isolated element by single-port measurement and as part of the filter by measuring the insertion loss. Figure 7 shows such characteristic filter transmission and how it is modified by a DC current

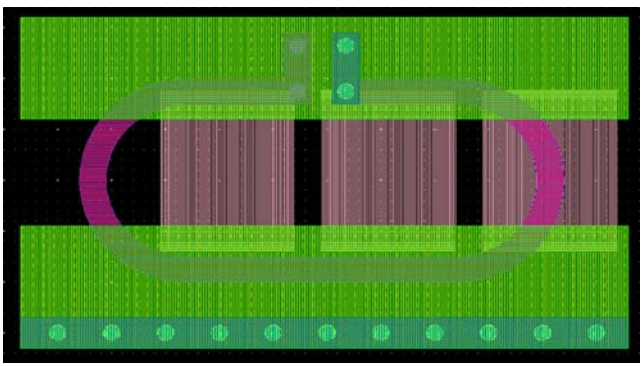

Fig. 5 Layout of line filter with buried oval inductor and three SMD capacitors on the front and back side. The size is 11.3×6.5 mm^2

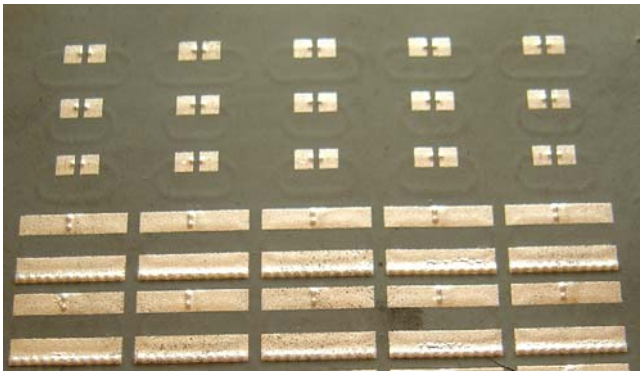

Fig. 6 Photograph of sintered ferrite multilayer plate with inductors for individual characterization (*top*) and for completion by SMD capacitors prior to assembly (*bottom*)

passing through the filter. At zero bias current it exhibits a pronounced peak at the cut-off frequency [20]

$$f_c = \frac{1}{\pi\sqrt{L \cdot C}} = 70\ \text{kHz} \qquad (1)$$

implying an inductance of 2.1 μH in close agreement with FEM. The sharpness of the cut-off peak agrees with the conductor DC resistance or loss of 20 mΩ or 2 W at 10 A, respectively.

4 Current capacity and DC insertion loss

Although adequate passive thermal management is needed to accept such conductor loss, this is not the limiting factor of the current capacity. It is rather the non-linear *B–H* curve of the ferrite in combination with the high flux density inside the small-sized device. This causes the deformations of the filter characteristics in Fig. 7. The magnetization of the material saturates with increasing bias current and the

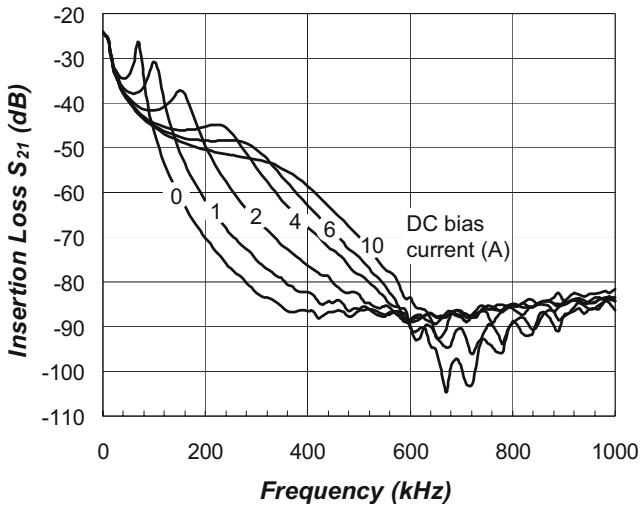

Fig. 7 Insertion loss of power line filter with LTCC integrated 2μH inductor and SMD capacitors. The effective permeability decreases and the cutoff frequency increases under a DC bias current

slope of the *B–H* curve, i.e. the small-signal permeability and the inductance decrease. The cut-off frequency of the filter consequently moves to higher frequency. To describe the effect in a finite element model, an analytic *B–H* curve (Fig. 8) was constructed in accordance with the measured hysteresis; it is characterized by a low-field permeability of 1,000, a saturation of 250 mT, and a high-field permeability of 14.

Since the inductance of a ferrite-embedded conductor is essentially independent of the shape of the coil due to the low reluctance path surrounding it, the FEM model reduced to a straight conductor line. A static simulation was run for each DC bias current first to obtain the DC magnetic field H_{DC}. For the subsequent harmonic simulation, *B–H* curves according to Fig. 8 were assigned with a certain discretization to the simplified volume elements which were shifted by the local DC field. As a result, an amplitude-dependent effective permeability $\mu_{eff}(H_{AC})$ is applied, which is varied locally by H_{DC}. The harmonic simulations finally deliver a fairly good reproduction (Fig. 9) of the measured inductance as determined from the cut-off frequencies. Beyond this approximate model, the *B–H* curve of Fig. 8 will likely depend on frequency, thus leading to a broadening of the filter characteristics near cut-off as seen in Fig. 7. It is concluded, that a careful balance is required in the design of integrated power inductors between the actually possible miniaturization and the limits set by the materials performance. In order to avoid magnetic saturation effects in soft ferrites, it is necessary to adjust device size and ferrite volume to materials characteristics.

Another device relevant ferrite property is electrical conductivity. Most good ferrites exhibit poor isolation; this

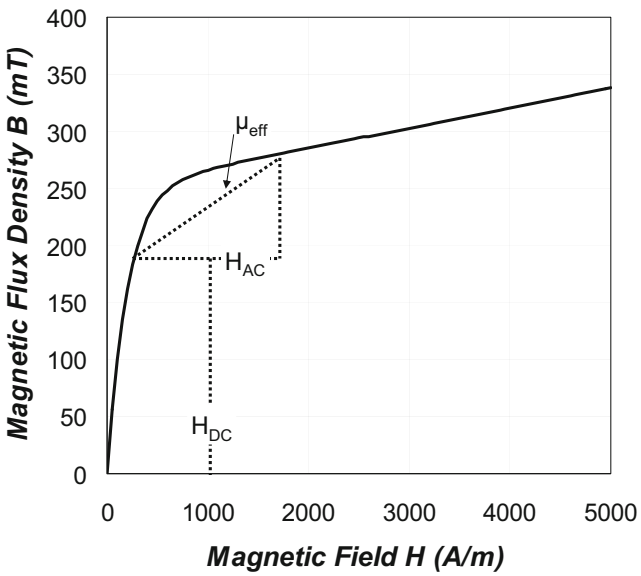

Fig. 8 *B–H* curve for FEM simulation of embedded inductors under DC bias current. The low and high field permeabilities are 1,000 and 14, respectively; the saturation flux density is 250 mT

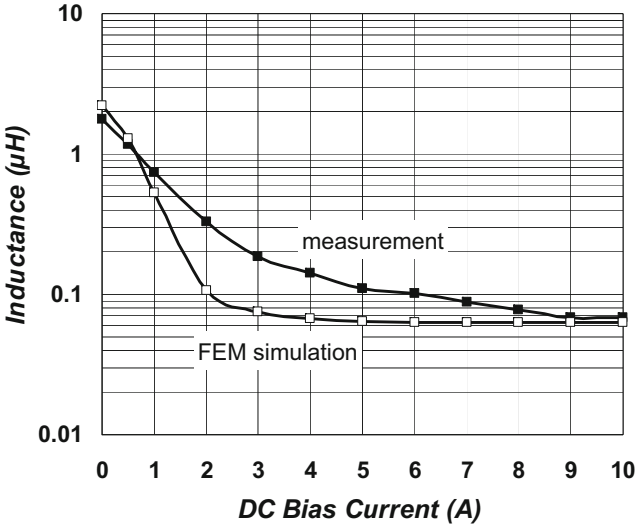

Fig. 9 Measured and FEM simulated inductance under DC bias current

correlation between high permeability and high conductivity was also confirmed for present LTCC MnZn ferrites under various sintering conditions. When the ground electrodes are directly attached to the ferrite layers of the inductor as in the present case, the ferrite may form a short between active ports and ground and its conductivity has large influence on the filter's DC insertion loss. The relation is given by

$$S_{21}(\mathrm{DC}) = \frac{2}{2 + R_C/50\Omega + 50\Omega/R_F + R_C/R_F} \qquad (2)$$

where R_C and R_F are the resistances of the conductor and the ferrite, respectively. Since R_C is typically in the 10 mΩ range while R_F varies from a few Ω up to more than a kΩ, the third term in the denominator is the relevant one. The insertion loss may therefore amount to 20 dB and more (see Fig. 7) or only 0.1 dB. This latter attractive situation has been always combined, however, with permeability near 200, i.e. reduced by factor of approximately three. To employ the full potential of the new MnZn ferrite with simultaneously good electrical isolation, the integration of ferrite tapes with dielectric tapes is essential.

5 Ferrite-dielectric integration

To avoid the resistive bypass to the SMD capacitors of the line filter, the outer ferrite layers were replaced by DuPont 951 dielectric cladding layers in an alternative design of the filter. This stack comprised 9 ferrite layers and 2 dielectric layers, each layer being 90μm thick after sintering. The insertion loss of the filter was indeed reduced to 1 dB due to the higher ferrite resistance of 200Ω but the cut-off frequency shifted from 70 to 180 kHz indicating also

reduced values of inductance and permeability of 0.3 μH and 70, respectively. The effect is caused by mechanical strain and band structure deformation in the ferrite due to the mismatch of the dielectric and ferrite thermal expansion coefficients. When the stack cools down after sintering from about 900 °C, opposite stress builds up in both materials. It can be estimated from elastic theory [21] according to

$$\sigma_1 d_1 = -\sigma_2 d_2 = \frac{(\alpha_1 - \alpha_2)\Delta T}{(1-\nu_1)/E_1 d_1 + (1-\nu_2)/E_2 d_2} \quad . \qquad (3)$$

The expression is being evaluated in Table 2 using elastic properties of both materials to yield a tensile stress in the ferrite of 160 MPa. The dielectric material is much thinner and therefore subject to even higher stress. Since these cladding layers are under compressive stress, no cracks develop and the samples remain intact.

The quenching of permeability by lattice deformation allows for simple designs of pressure sensors and variable inductors (variometers) without moving mechanical parts. Figure 10 shows the inductance of two inductors measured by an impedance analyzer when a mechanical workbench exerts increasing uniaxial pressure on the inductor and a force measuring element. A 25% change occurs for approximately 20 MPa. This compares well with the 90% change under built-in 160 MPa mentioned before.

6 Conclusion

MnZn ferrite tapes have been successfully developed for integration into the LTCC technology. Dense sintering at 900 °C was achieved by high energy powder milling, use of BBSZ glass as sintering additive, and atmospherically controlled sintering. Compared to high temperature sintered material, the amplitude permeability is reduced to 500–700 by smaller grain size. Hysteresis losses are also more pronounced but completely compensated by weak eddy current losses. By variation of the detailed sintering conditions, a positive correlation between permeability and electrical conductivity is found. Therefore additional electrical insulation must be taken into account in the device design, when high permeability is needed.

Embedded 2μH inductors with a single turn of two parallel conductors screen printed on neighbouring ferrite layers achieved 10 A current capacity. They were successfully used in power line filters for cut-off below 100 kHz. Strong changes observed in the filter characteristics under external pressure appear useful for the construction of simple variometers and pressure sensors.

The high flux density in miniaturized LTCC devices drives the material into magnetic saturation under operational conditions where larger discrete devices exhibit stable performance. Therefore less ambitious design rules need to be developed in future to balance material performance limits and device shrinkage. Most important, however, will be the availability of thermally matched dielectric base tapes to integrate good electrical isolation into a ferrite multilayer without sacrificing its magnetic performance by strain.

In summary, the new LTCC ferrite is performing well in first inductive devices as a stand-alone material. Also further refinement in design and processing has been identified, particularly the integration of matched materials, to make the advantages of the material fully accessible.

Table 2 Calculation of stress in LTCC-integrated MnZn ferrite using Eq. 3.

Quantity		Unit	Value in material 1 (MnZn ferrite)	Value in material 2 (dielectric)
Thermal expansion	α	ppm/K	11.5	5.8
Temperature interval	ΔT	K	850	850
Poisson ratio	ν	–	0.17	0.17
Young's modulus	E	GPa	90–150	152
Total thickness	d	μm	810	180
Calculated stress	σ	MPa (10 bar)	160 (Tension)	−720 (Compression)

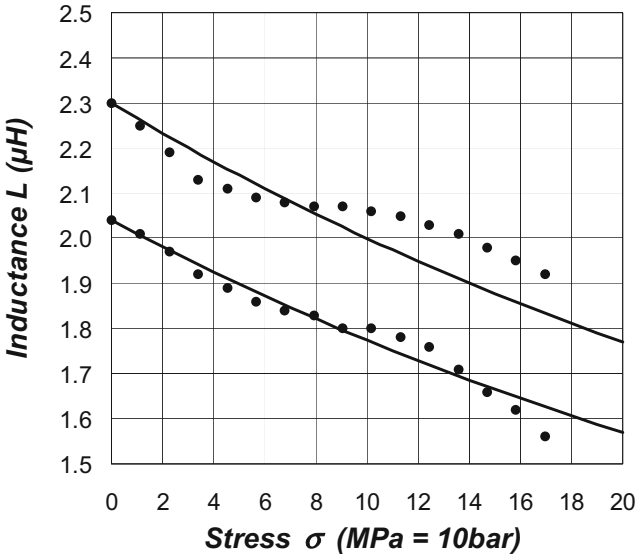

Fig. 10 Measured inductance loss of two different MnZn ferrite integrated inductors under mechanically applied stress (*dots*). *Solid lines* indicate the relation $L(\sigma) = L(0)/(1 + k\sigma)$, where k is 3×10^{-5}/MPa

Acknowledgment This work was supported by the Bundesministerium fuer Bildung und Forschung (BMBF) under grant no. 03X4503B, project NIKOL.

References

1. H. Jiang, Y. Wang, J.-L.A. Yeh, N.C. Tien, IEEE Trans. Microwave Theor. Tech. **48**, 2415 (2000)
2. J. Zou, C. Liu, D.R. Trainor, J. Chen, J.E. Schutt-Ainé, P.L. Chapman, IEEE Trans. Microwave Theor. Tech. **51**, 1067 (2003)
3. E. Waffenschmidt, 35th Annual IEEE Power Electronics Specialists Conf. (Aachen, Germany, 2004), p. 4546
4. M. Ludwig, M. Duffy, T. O'Donnell, P. McCloskey, S.C. Ó Mathùna, IEEE Trans. Power Electronics **18**, 937 (2003)
5. S.S.M. Chan, H.S.-H. Chung, Y.S. Lee, IEEE Trans. Power Electronics **22**, 291 (2007)
6. R. Karmazin, O. Dernovsek, N. Ilkov, W. Wersing, A. Roosen, M. Hagymasi, J. Eur. Ceram. Soc. **25**, 2029 (2005)
7. M. Matters-Kammerer, U. Mackens, K. Reimann, R. Pietig, D. Hennings, B. Schreinemacher, R. Mauczok, S. Gruhlke, C. Martiny, Microelectronics Reliability **46**, 134 (2006)
8. S. Barth, F. Bechtold, E. Müller, J. Mürbe, J. Töpfer, CICMT 2005, Proceedings 1st IMAPS/ACerS Int. Conf. and Exhibition on Ceramic Interconnect and Ceramic Microsystems Technologies (Baltimore, USA, 10–13 April 2005)
9. R. Hahn, G. Sommer, I. Dörr, S. Schwerzel, H. Reichl, Advancing Microelectronics **33**, 8 (2006), November/December
10. M.H.F. Lim, Z. Liang, J.D. van Wyk, IEEE Trans. Compon. Packag. Technol. **30**, 170 (2007)
11. W.G. Hurley, M.C. Duffy, IEEE Trans. Magnetics **31**, 2416 (1995)
12. L. Zhao, J.D. van Wyk, IEEE Trans. Circuits Syst. **51**, 2325 (2004)
13. R.L. Wahlers, C.Y.D. Huang, M.R. Heinz, A.H. Feingold, J. Bielawski, G. Slama, Proc. 2002 Int. Symp. Microelectronics, IMAPS Int. Microelectronics and Packaging Soc. (Denver, USA, 4–6 Sep. 2002), p. 76
14. G. Slama, *Power Electronics Technology*, Jan. 2003, p. 30.
15. Q. Yu, H. Wang, Y. Geng, Z. Liu, Proc. 6th World Congr. Intelligent Control and Automation (Dallan, China, 21–23 June 2006), p. 5272
16. Fi328 by Vogt-electronic, Obernzell, Germany and N27 by EPCOS AG, Munich, Germany
17. Soft Ferrites and Accessories, Data Handbook (Ferroxcube International Holding B.V. 2004)
18. K. Küpfmüller, *Theoretische Elektrotechnik* (Springer, Berlin, 1973), p. 315
19. ANSYS, Inc., Southpointe, 275 Technology Drive, Canonsburg, PA 15317, http://www.ansys.com
20. D.M. Pozar, *Microwave Engineering* (Wiley, New York, 1998), p. 433
21. L.D. Landau, E.M. Lifschitz, *Lehrbuch der Theoretischen Physik, Elastizitätstheorie* (Akademie-Verlag, Berlin, 1975), p. 17